

applications, such as designing a new manipulator or using an existing robotic system.

Hybrid Modeling and Analysis Method for Dynamic Coupling of Space Robots

WENFU XU, Member, IEEE

JIANQING PENG

HIT Shenzhen Graduate School

Shenzhen, China

BIN LIANG, Member, IEEE

Tsinghua University

Beijing, China

ZONGGAO MU

HIT Shenzhen Graduate School

Shenzhen, China

Resolving linear and angular momentum conservation equations in different ways, a hybrid method was proposed to model and analyze the dynamic coupling of a space robotic system. This method dealt with the coupling problems for the base's centroid position at the position level and attitude at the velocity level. Based on the base centroid virtual manipulator concept, the coupled space was addressed to represent the base's centroid position coupling. For different cases, the reachable coupled space, attitude-constrained coupled space, and free coupled space were defined. However, the coupling for the base's velocities was decomposed into joint-to-base rotation, joint-to-base translation, end-to-base rotation, and end-to-base translation coupling types. The dependence of the rotation and translation coupling was revealed, and the coupling factors were determined to measure the coupling degree. Then, the coupling effect for different loads, installation positions, and joint configurations was analyzed. Coupled maps were established to plan the trajectory for minimizing disturbance. Compared with previous works, dynamic coupling at the position level avoids the singularity problem for solving differential equations; at the velocity level, each type of coupling motion was separately modeled and analyzed for different requirements. The proposed method is useful for practical

Manuscript received October 7, 2014; revised March 29, 2015; released for publication July 15, 2015.

DOI. No. 10.1109/TAES.2015.140752.

Refereeing of this contribution was handled by S. Karaman.

This work was supported in part by the National Natural Science Foundation of China (Grant No. 61175098 and 61573116) and the Basic Research Program of Shenzhen (JCYJ20140417172417095, JCYJ20140417172417129).

Authors' addresses: W. Xu, J. Peng, Z. Mu, School of Mechanical Engineering and Automation, Harbin Institute of Technology Shenzhen Graduate School, Shenzhen 518055, China, E-mail: (wfxu@hit.edu.cn); B. Liang, Department of Automation, Tsinghua University, Beijing 100854, China.

I. INTRODUCTION

Space robots will play important roles in future space activities, such as inspecting, repairing, upgrading, and refueling spacecraft [1–9]. They have the potential to extend satellite life, enhance the capability of space systems, reduce operation costs, and clean up space debris.

Because of dynamic interaction, the motion of a manipulator alters the position and attitude of the base; furthermore, the end-effectors lose the desired target pose (position and attitude) because of the motion of the base [10, 11]. This phenomenon is called dynamic coupling. It complicates the trajectory planning and control of a space robotic system [12, 13], especially when the mass and inertia of a space manipulator are not negligible in comparison to the base. Without considering the dynamic coupling, the control methods for the space manipulator will not be valid or have high control accuracy and good dynamic performance. Therefore, in the past two decades, the scholars have proposed some important modeling and control concepts [14]. Ma et al. [15] derived general dynamic equations for a complex space system and developed the simulation facility MDSF (a generic development and simulation facility), which is a good reference because it has been validated using the true flight data of space manipulators on the International Space Station. Vafa and Dubowsky [16] presented a virtual manipulator (VM) approach and used it to simplify the kinematics and analyze the workspace of a space robot. Liang et al. [17] proposed the dynamically equivalent manipulator. Umetani and Yoshida [18] presented the generalized Jacobian matrix (GJM) and resolved the motion control method. Based on the GJM, a variety of control schemes developed for a fixed-base manipulator can be extended to a space robot by using only the GJM to replace the traditional Jacobian matrix. Nakamura and Mukherjee [19] employed the bidirectional approach to plan the path for controlling both the manipulator configuration and the spacecraft orientation. Yoshida et al. addressed the zero reaction maneuver concept [20] and demonstrated it on the ETS-VII [21]. Xu et al. [22] proposed a method based on the particle swarm optimization algorithm to plan the Cartesian point-to-point path of the end-effector and adjust the base attitude at the same time. The authors [23] also developed a unified multidomain modeling and simulation system to analyze the dynamic performances of multiphysics interactions among mechanical, electrical, electronic, control, and so on.

To thoroughly understand and effectively use the dynamic coupling, Xu and Shum [24] derived the theoretical model for a space robotic system, and Bergerman et al. [25] focused on underactuated manipulators. Bergerman et al. [26] also proposed the coupling factor to illustrate the motion and force

dependencies and represent the degree of the dynamic coupling. This concept was successfully applied for the motion planning and control of a free-floating space robot [27–31]. The key of the method is to solve the conservation equation of the system's momentum, including the linear and angular momentum. It is required to solve the differential kinematic equations, which contain all state variables of the system. Therefore, the computation load is relatively large, and complex singularity problems exist. The linear and angular momentum conservation equations have different characteristics. The former is a holonomic constraint and can be integrated to obtain the relationship of the position. The latter is a nonholonomic constraint; i.e., the differential equation is nonintegrable.

In this paper, we present a hybrid method to model the dynamic coupling and define the corresponding coupling factors by handling the linear and angular momentum conservation equations in different ways. The expression of the base's centroid position is obtained by analytically integrating the linear momentum conservation equation. Then, the coupling effect on the base centroid generated by the manipulator is analyzed at the position level, directly reflecting the position relationship. The variation range of the base centroid is determined according to the workspace of the manipulator. The calculation of the Jacobian matrix and its inverse is avoided. Furthermore, the coupling motion of the base attitude is derived by solving the angular momentum conservation and eliminating the holonomic constraints. Hence, the coupling effect on the base attitude is analyzed using velocity-level coupling model with lower dimension, also reducing the computation cost.

The remainder of this paper is organized as follows. In Section II, we derive the general kinematics and momentum conservation equations of a free-floating space robotic system, establishing the theoretical foundation for dynamic coupling modeling and analysis. In Section III, we decompose the dynamic coupling problem into two subproblems for the centroid position and attitude of the base, based on different characteristics of the linear and angular momentum. Then, we propose the hybrid dynamic coupling modeling concept, i.e., position-level and velocity-level modeling for the centroid position and attitude, respectively. Section IV derives the corresponding coupling factor for the hybrid method. In Section V, we analyze the dynamic coupling effects for different loads and the mounting pose of the manipulator. The coupling maps are also established to intuitively illustrate the coupling degree about the joint configurations. In the final section, we offer a discussion and conclusion of the study.

II. MODELING OF A FREE-FLOATING SPACE ROBOT

A space robotic system is composed of a carrier spacecraft (called the space base or base) and an n -degrees of freedom (DOF) manipulator (called the space manipulator). Fig. 1 shows a general model of a space

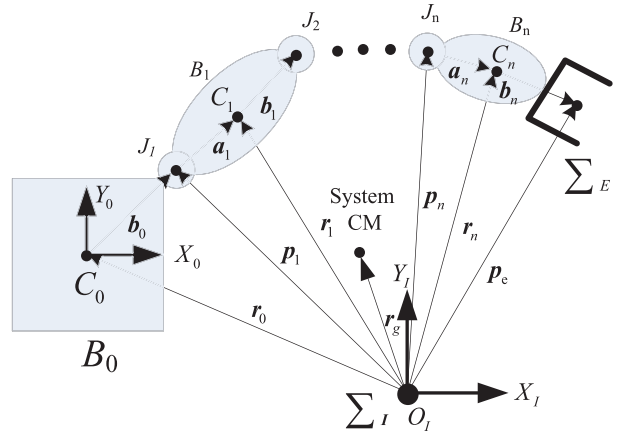


Fig. 1. General model of serial space robot.

robotic system, which is regarded as an $n + 1$ serial link system connected with n -DOF active joints. B_0 denotes the satellite main body; B_i ($i = 1, \dots, n$) denotes the i th link of the manipulator; \mathbf{r}_i ($i = 0, \dots, n$) is the position vector of B_i 's centroid; \mathbf{I}_i ($i = 0, \dots, n$) is the inertia matrix of B_i with respect to its center of mass (CM); \mathbf{k}_i and \mathbf{p}_i ($i = 1, \dots, n$) are, respectively, the rotation vector and the position vector of the i th joint; \mathbf{r}_g is the position vector of the system's CM; \mathbf{p}_e is the position vector of the end-effector; \mathbf{a}_i and \mathbf{b}_i are, respectively, the position vectors from the i th joint to the B_i 's CM and from the B_i 's CM to the $(i + 1)$ th joint; and $\mathbf{l}_i = \mathbf{a}_i + \mathbf{b}_i$. The mass of B_i and the total mass of the system are denoted by m_i and M , respectively.

A. General Kinematics Equations

Based on Fig. 1, the differential kinematic equation of a space robotic system can be determined as follows:

$$\begin{bmatrix} \mathbf{v}_e \\ \boldsymbol{\omega}_e \end{bmatrix} = \mathbf{J}_b \begin{bmatrix} \mathbf{v}_0 \\ \boldsymbol{\omega}_0 \end{bmatrix} + \mathbf{J}_m \dot{\Theta} \quad (1)$$

where \mathbf{v}_e and $\boldsymbol{\omega}_e$ are the linear and the angular velocities of the base, respectively; \mathbf{v}_0 and $\boldsymbol{\omega}_0$ are the linear and angular velocities of the end-effector, respectively; Θ is the joint angle vector (i.e., $\Theta = [\theta_1, \dots, \theta_n]$); and \mathbf{J}_b and \mathbf{J}_m are the Jacobian matrices mapping the velocities of the base and the manipulator to those of the end-effector, respectively. \mathbf{J}_b and \mathbf{J}_m are defined as follows:

$$\mathbf{J}_b = \begin{pmatrix} \mathbf{E} & -\mathbf{p}_{0e}^\times \\ \mathbf{O} & \mathbf{E} \end{pmatrix} = \begin{bmatrix} \mathbf{J}_{bv} & \mathbf{J}_{bw} \end{bmatrix} \in \mathbf{R}^{6 \times 6}, \quad \mathbf{p}_{0e} = \mathbf{p}_e - \mathbf{r}_0 \quad (2)$$

$$\begin{aligned} \mathbf{J}_m &= \begin{bmatrix} \mathbf{k}_1 \times (\mathbf{p}_e - \mathbf{p}_1) & \dots & \mathbf{k}_n \times (\mathbf{p}_e - \mathbf{p}_n) \\ \mathbf{k}_1 & \dots & \mathbf{k}_n \end{bmatrix} \\ &= \begin{bmatrix} \mathbf{J}_{mv} & \mathbf{J}_{mw} \end{bmatrix} \in \mathbf{R}^{6 \times n} \end{aligned} \quad (3)$$

where \mathbf{p}_{0e}^\times is the skew-symmetric matrix determined by \mathbf{p}_{0e} and \mathbf{J}_{bv} , \mathbf{J}_{bw} and \mathbf{J}_{mv} , \mathbf{J}_{mw} are the submatrices of \mathbf{J}_b corresponding to the linear and angular velocities,

respectively. Matrices \mathbf{E} and \mathbf{O} are the identity and zeros matrices, respectively.

B. Momentum Equations for Free-Floating Mode

External forces and torques acting on the free-floating system are negligible. Then, the linear and angular momentums of the system are conserved. With the assumption that their initial values are zeros, the conservation equations are written as follows:

$$\mathbf{P} = m_0 \mathbf{v}_0 + \sum_{i=1}^n m_i \dot{\mathbf{r}}_i = \mathbf{O} \quad (4)$$

$$\mathbf{L} = (\mathbf{I}_0 \boldsymbol{\omega}_0 + \mathbf{r}_0 \times m_0 \dot{\mathbf{r}}_0) + \sum_{i=1}^n (\mathbf{I}_i \boldsymbol{\omega}_i + \mathbf{r}_i \times m_i \dot{\mathbf{r}}_i) = \mathbf{O} \quad (5)$$

where \mathbf{P} and \mathbf{L} denote the linear and angular momentums, respectively. Equations (4) and (5) can be further simplified and written in the matrix form:

$$\begin{pmatrix} M\mathbf{E} & M(\mathbf{r}_{0g}^\times)^T \\ M\mathbf{r}_g^\times & \mathbf{I}_w \end{pmatrix} \begin{bmatrix} \mathbf{v}_0 \\ \boldsymbol{\omega}_0 \end{bmatrix} + \begin{bmatrix} \mathbf{J}_{Tw} \\ \mathbf{I}_\phi \end{bmatrix} \dot{\boldsymbol{\Theta}} = \begin{bmatrix} \mathbf{O} \\ \mathbf{O} \end{bmatrix} \quad (6)$$

where

$$\mathbf{I}_w = \mathbf{I}_0 + \sum_{i=1}^n (\mathbf{I}_i + m_i \mathbf{r}_i^\times (\mathbf{r}_{0i}^\times)^T) \quad (7)$$

$$\mathbf{J}_{Tw} = \sum_{i=1}^n (m_i \mathbf{J}_{Ti}) \in \mathbf{R}^{3 \times n} \quad (8)$$

$$\mathbf{I}_\phi = \sum_{i=1}^n (\mathbf{I}_i \mathbf{J}_{Ri} + m_i \mathbf{r}_i^\times \mathbf{J}_{Ti}) \quad (9)$$

$$\mathbf{J}_{Ti} = [\mathbf{z}_1 \times (\mathbf{r}_i - \mathbf{p}_1), \dots, \mathbf{z}_i \times (\mathbf{r}_i - \mathbf{p}_i), 0, \dots, 0] \in \mathbf{R}^{3 \times n} \quad (10)$$

$$\mathbf{J}_{Ri} = [\mathbf{z}_1, \dots, \mathbf{z}_i, 0, \dots, 0] \quad (11)$$

$$\mathbf{r}_{0g} = \mathbf{r}_g - \mathbf{r}_0, \quad \mathbf{r}_{0i} = \mathbf{r}_i - \mathbf{r}_0 \quad (12)$$

Equation (6) can be further written as follows:

$$\mathbf{H}_b \dot{\mathbf{x}}_b + \mathbf{H}_{bm} \dot{\boldsymbol{\Theta}} = \mathbf{O} \quad (13)$$

The matrices \mathbf{H}_b and \mathbf{H}_{bm} are the inertia matrix of the base and the coupling inertia matrix, respectively. They are defined as follows:

$$\mathbf{H}_b = \begin{pmatrix} M\mathbf{E} & M(\mathbf{r}_{0g}^\times)^T \\ M\mathbf{r}_g^\times & \mathbf{I}_w \end{pmatrix} \in \mathbf{R}^{6 \times 6} \quad (14)$$

$$\mathbf{H}_{bm} = \begin{bmatrix} \mathbf{J}_{Tw} \\ \mathbf{I}_\phi \end{bmatrix} \in \mathbf{R}^{6 \times n} \quad (15)$$

III. Hybrid Dynamic Coupling Modeling Method

A. Coupling Movements Decomposition

Instead of directly solving the momentum conservation equation in (13), we handled the linear and angular

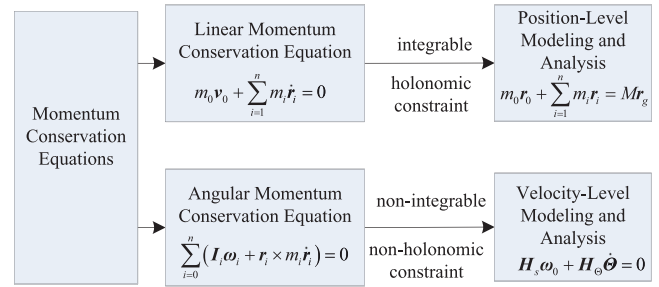


Fig. 2. Coupling movement decomposition concept.

momentum conservations in different ways because they had different characteristics. The linear momentum conservation equation, i.e., (4), is integrable. Hence, it is a holonomic constraint. However, the angular momentum conservation equation is a nonholonomic constraint.

Based on the holonomic constraint, the centroid position of the base can be determined by current joint angles, and its linear velocity can be determined by current joint angles and rates. That is to say, the coupling effect on the centroid generated by the manipulator can be analyzed at both the velocity and the position level. The position-level analysis has several advantages over the velocity-level analysis. The former directly reflects the position relationship and can be used to determine the variation range of the base centroid according to the manipulator workspace. Moreover, the calculation of the Jacobian matrix and its inverse is avoided. However, the attitude angle and angular velocity of the base are constrained by the angular momentum conservation equation, which cannot be resolved analytically. Hence, the attitude motion of the base can only be analyzed at the velocity level.

Therefore, we decompose the dynamic coupling modeling problem into two subproblems: position-level coupling modeling for the base centroid position and velocity-level coupling modeling for the base attitude. The decomposition concept is shown in Fig. 2.

B. Position-Level Modeling for Base Centroid Coupling

1) *Base Centroid VM Concept*: The position vectors of each body satisfy the following condition:

$$m_0 \mathbf{r}_0 + \sum_{i=1}^n m_i \mathbf{r}_i = M \mathbf{r}_g \quad (16)$$

Substituting the position vectors of B_i into (16), the CM of the base is determined by the following:

$$\mathbf{r}_0 = \mathbf{r}_g - \frac{\sum_{i=1}^n m_i \mathbf{b}_0}{M} - \frac{\sum_{i=1}^n m_i \left(\sum_{j=1}^{i-1} (\mathbf{a}_j + \mathbf{b}_j) + \mathbf{a}_i \right)}{M} \quad (17)$$

According to (17), the position vector from the system's CM to the base's CM is as follows:

$$\mathbf{r}_{g0} = -\mathbf{r}_\Sigma(\mathbf{q}) \quad (18)$$

TABLE I
Comparison of VM and BCVM

Name	VM	BCVM
End-effector	$\hat{p}_e^{\text{VM}} = \mathbf{r}_g + \hat{\mathbf{b}}_0 + \sum_{i=1}^n (\hat{\mathbf{a}}_i + \hat{\mathbf{b}}_i)$	$\tilde{p}_e^{\text{BCVM}} = \tilde{\mathbf{b}}_0 + \sum_{i=1}^{n-1} (\tilde{\mathbf{a}}_i + \tilde{\mathbf{b}}_i) + \tilde{\mathbf{a}}_n$
Virtual link	$\begin{cases} \hat{\mathbf{b}}_i = \frac{\sum_{q=0}^i m_q}{M} \mathbf{b}_i & (i = 1, \dots, n) \\ \hat{\mathbf{a}}_i = \frac{\sum_{q=0}^{i-1} m_q}{M} \mathbf{a}_i \end{cases}$	$\begin{cases} \tilde{\mathbf{a}}_i = \frac{\sum_{q=i}^n m_q}{M} \mathbf{a}_i & (i = 1, 2, \dots, n) \\ \tilde{\mathbf{b}}_i = \frac{\sum_{q=i+1}^n m_q}{M} \mathbf{b}_i & (i = 0, 1, \dots, n-1) \end{cases}$

where

$$\mathbf{r}_{g0} = -\mathbf{r}_{0g} = \mathbf{r}_0 - \mathbf{r}_g \quad (19)$$

$$\mathbf{r}_\Sigma(\mathbf{q}) = \frac{\sum_{i=1}^n m_i \mathbf{b}_0}{M} + \frac{\sum_{i=1}^n m_i \left(\sum_{j=1}^{i-1} (\mathbf{a}_j + \mathbf{b}_j) + \mathbf{a}_i \right)}{M} \quad (20)$$

If the inertia frame is created at the system's CM, $\mathbf{r}_g = \mathbf{O}$ and $\mathbf{r}_{g0} = \mathbf{r}_0$. Equation (20) can be rewritten as follows:

$$\mathbf{r}_\Sigma(\mathbf{q}) = \tilde{\mathbf{b}}_0 + \sum_{i=1}^{n-1} (\tilde{\mathbf{a}}_i + \tilde{\mathbf{b}}_i) + \tilde{\mathbf{a}}_n \quad (21)$$

where

$$\begin{cases} \tilde{\mathbf{a}}_i = \frac{\sum_{q=i}^n m_q}{M} \mathbf{a}_i & (i = 1, 2, \dots, n) \\ \tilde{\mathbf{b}}_i = \frac{\sum_{q=i+1}^n m_q}{M} \mathbf{b}_i & (i = 0, 1, \dots, n-1) \end{cases} \quad (22)$$

According to (22), vectors $\tilde{\mathbf{a}}_i$ and $\tilde{\mathbf{b}}_i$ are aligned with vectors \mathbf{a}_i and \mathbf{b}_i , respectively. Their lengths are constantly proportional to those of the corresponding vectors. We set

$$\tilde{l}_i = \tilde{\mathbf{a}}_i + \tilde{\mathbf{b}}_i \quad (i = 1, 2, \dots, n-1) \quad (23)$$

and (18) becomes the following:

$$\mathbf{r}_{g0} = -\mathbf{r}_\Sigma(\mathbf{q}) = -\left(\tilde{\mathbf{b}}_0 + \sum_{i=1}^{n-1} \tilde{l}_i + \tilde{\mathbf{a}}_n \right) \quad (24)$$

These vectors, i.e., $\tilde{\mathbf{b}}_0$, \tilde{l}_i ($i = 1, 2, \dots, n-1$), and $\tilde{\mathbf{a}}_n$, form an equivalent n -DOF manipulator, shown in Fig. 3.

The link lengths of the manipulator are denoted as \tilde{l}_i ($i = 1, \dots, n-1$), and $\tilde{\mathbf{a}}_n$. The rotation direction of each joint of the equivalent manipulator is the same as the corresponding joint axis. This equivalent manipulator is the so-called base centroid virtual manipulator, or BCVM for short. It has the following characteristics:

1) The lengths of the equivalent manipulator's link, i.e., $\tilde{\mathbf{b}}_0$, \tilde{l}_i , and $\tilde{\mathbf{a}}_n$, remain constant and do not change as the manipulator moves.

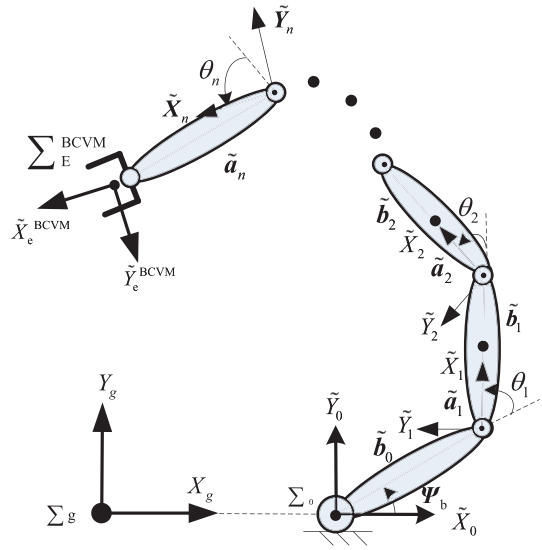


Fig. 3. BCVM model of free-floating space robot.

2) The axis of the i th joint of the equivalent manipulator is always parallel to the i th axis of the real manipulator joint.

3) The amount of rotation of the i th joint of the equivalent manipulator is equal to that of the i th joint of the real manipulator.

The concept of the BCVM comes from previous works by Vafa and Dubowsky [16]. In our study, the difference is that the proposed concept focuses on the position vector from the system centroid to the base centroid. A more detailed comparison of VM and BCVM is shown in Table I.

2) Coupling Effect for Base Centroid

Position: According to Fig. 3, the position vector of the BCVM's end-effector is as follows:

$$\tilde{p}_e^{\text{BCVM}} = \left[\tilde{\mathbf{b}}_0 + \sum_{i=1}^{n-1} (\tilde{\mathbf{a}}_i + \tilde{\mathbf{b}}_i) + \tilde{\mathbf{a}}_n \right] = \text{fkine}(\Psi_0, \Theta) \quad (25)$$

where fkine() represent the forward kinematical equation of the VM and Ψ_0 is the attitude of the base. The position vectors of the base centroid and the end-effector of the BCVM satisfy the following relationship:

$$\tilde{p}_e^{\text{BCVM}} + \mathbf{r}_{g0} = \mathbf{O} \quad (26)$$

That is to say,

$$\begin{aligned} \mathbf{r}_{g0} &= -\tilde{\mathbf{p}}_e^{\text{BCVM}} = -A_0 \left({}^0\tilde{\mathbf{b}}_0 + \sum_{i=1}^{n-1} {}^0A_i {}^i\tilde{\mathbf{l}}_i + {}^0A_n {}^n\tilde{\mathbf{a}}_n \right) \\ &= -A_0 \cdot {}^0\text{fkine}(\Theta) \end{aligned} \quad (27)$$

where A_0 is the attitude matrix of the base relative to the inertial frame. The superscript i ($i = 0, \dots, n$) denotes the frame used to describe the vectors. Equation (27) shows that the movement range of the base centroid can be determined by analyzing the workspace of the BCVM.

According to different attitude control modes, the workspace of a space robot was classified into the following three types [16, 32]: the maximum reachable workspace (RWS), the attitude-constrained workspace (CWS), and the free workspace (FWS, also called the guaranteed workspace). These concepts [32] are extended here to express the coupled motion of the base centroid. Three types of coupled space are defined: the reachable coupled space (RCS), the attitude-constrained coupled space (CCS), and the free coupled space (FCS).

The RCS is the maximum envelope of the base centroid in case of no special constraints on the base attitude and the manipulator joints except the mechanical limitations. Then, the distance from the system's CM to the end-effector of the BCVM is

$$\begin{aligned} \|\mathbf{r}_{g0}\| &= \| -A_0 \cdot {}^0\text{fkine}(\Theta) \| = \| {}^0\text{fkine}(\Theta) \| \\ &= \left\| \left({}^0\tilde{\mathbf{b}}_0 + \sum_{i=1}^{n-1} {}^0A_i \left({}^i\tilde{\mathbf{a}}_i + {}^i\tilde{\mathbf{b}}_i \right) + {}^0A_n {}^n\tilde{\mathbf{a}}_n \right) \right\| \end{aligned} \quad (28)$$

where 0A_i is the attitude matrix of the i th frame relative to the base frame. Equation (28) shows that the distance from the system's CM to the base centroid is independent on the base attitude Ψ_0 . For a given configuration Θ , there are infinite potential positions of the base centroid. These points lie on a spherical surface whose center is the system's CM. Then, the calculation of the radius R_{RCS} can be simplified as follows:

$$R_{\text{RCS}} = \max_{\Theta} (\| {}^0\text{fkine}(\Theta) \|), \quad \text{where } \Theta \in [\Theta_{\min}, \Theta_{\max}] \quad (29)$$

Here, Θ_{\min} and Θ_{\max} are the minimum and maximum of the joint angles, respectively. The position vector of the RCS's center is denoted by the following:

$$\mathbf{O}_{\text{RCS}} = \mathbf{r}_g \quad (30)$$

The CCS is a reachable envelope when the base's attitude is fixed at a certain value, i.e., $\Psi_b = \Psi_0$. Correspondingly, the attitude transform matrix A_0 is a constant matrix, and vector $A_0 \cdot {}^0\tilde{\mathbf{b}}_0$ is a constant vector. From (27), the position of the base centroid with respect to a fixed point P located at $\mathbf{r}_g + A_0 {}^0\tilde{\mathbf{b}}_0$ is as follows:

$$\mathbf{r}_{g0} + A_0 \cdot {}^0\tilde{\mathbf{b}}_0 = -A_0 \left(\sum_{i=1}^{n-1} {}^0A_i \left({}^i\tilde{\mathbf{a}}_i + {}^i\tilde{\mathbf{b}}_i \right) + {}^0A_n {}^n\tilde{\mathbf{a}}_n \right) \quad (31)$$

The distance is then as follows:

$$\begin{aligned} \|\mathbf{r}_{g0} + A_0 \cdot {}^0\tilde{\mathbf{b}}_0\| &= \left\| -A_0 \left(\sum_{i=1}^{n-1} {}^0A_i \left({}^i\tilde{\mathbf{a}}_i + {}^i\tilde{\mathbf{b}}_i \right) + {}^0A_n {}^n\tilde{\mathbf{a}}_n \right) \right\| \\ &= \left\| \left(\sum_{i=1}^{n-1} {}^0A_i \left({}^i\tilde{\mathbf{a}}_i + {}^i\tilde{\mathbf{b}}_i \right) + {}^0A_n {}^n\tilde{\mathbf{a}}_n \right) \right\| \end{aligned} \quad (32)$$

Therefore, the CCS is a sphere whose center is $\mathbf{r}_g + A_0 \cdot {}^0\tilde{\mathbf{b}}_0$, and the radius is

$$R_{\text{CCS}} = \max_{\Theta} \left(\left\| \left(\sum_{i=1}^{n-1} {}^0A_i \left({}^i\tilde{\mathbf{a}}_i + {}^i\tilde{\mathbf{b}}_i \right) + {}^0A_n {}^n\tilde{\mathbf{a}}_n \right) \right\| \right) \quad (33)$$

where $\Theta \in [\Theta_{\min}, \Theta_{\max}]$. Equations (31) and (32) show that the length of the CCS's radius is also independent of the given base attitude Ψ_0 . For different CCSs (determined by different base attitudes), their radiiuses are the same. The only difference between them is the position of the center:

$$\mathbf{O}_{\text{CWS}} = \mathbf{r}_g + A_0 {}^0\tilde{\mathbf{b}}_0 \quad (34)$$

The FCS is the region in which the base centroid is always reachable, without regard for the vehicle orientation. It can be shown that the FCS is equal to the intersection of all CCSs for all possible fixed vehicle orientations:

$$\text{FCS} = \bigcap_{\Psi_b} \text{CCS}(\Psi_b), \quad \text{where } \Psi_b \in [\Psi_{\min}, \Psi_{\max}] \quad (35)$$

According to the preceding definitions, the CWS is a sphere whose center is the system's CM, i.e., the point fixed at \mathbf{r}_g , and the radius is as follows:

$$R_{\text{FCS}} = R_{\text{CCS}} - \left(\| {}^0\tilde{\mathbf{b}}_0 \| \right) \quad (36)$$

The position vector of the FCS's center is denoted by the following:

$$\mathbf{O}_{\text{FCS}} = \mathbf{r}_g \quad (37)$$

Based on the position-level modeling concept, the coupling effect on the base centroid position caused by the manipulator is represented by the coupled workspace, including RCS, CCS, and FCS for different cases.

Three types of workspace and coupled space are shown in Fig. 4 that are related to the planar space robotic system introduced later in Fig. 5 and Table II.

C. Velocity-Level Modeling for Base Attitude Coupling

1) *Angular Momentum Conservation*: Substituting the velocities of B_i into (5), the angular momentum equation can be defined as follows:

$$\mathbf{L} = [M\mathbf{r}_{0g} \times \mathbf{I}_w] \begin{bmatrix} \mathbf{v}_0 \\ \boldsymbol{\omega}_0 \end{bmatrix} + \mathbf{I}_\phi \dot{\boldsymbol{\Theta}} \quad (38)$$

Based on (26), we know the following:

$$\mathbf{v}_0 = -\tilde{\mathbf{v}}_e \quad (39)$$

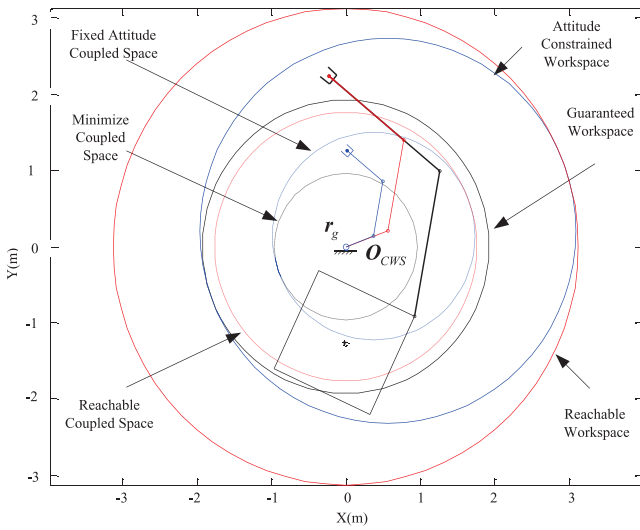


Fig. 4. Three types of workspace and coupled space.

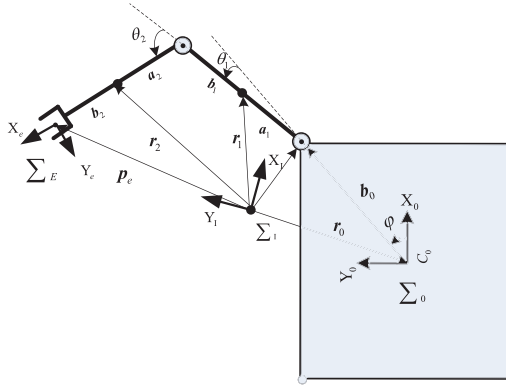


Fig. 5. Planar space manipulator.

TABLE II
Mass Properties of Space Robotic System

Name	Mass (kg)	$i\mathbf{a}_i$ (m)	$i\mathbf{b}_i$ (m)	I_i (kg.m 2)
Base	300	0	0	1.0
B_1	25	0.97	0	0.97
B_2	25	0.97	0	0.97
B_L	$m_L \in [0, 150]$	—	—	—

Differentiating both sides of (25) yields the following:

$$\tilde{\mathbf{v}}_e = \dot{\tilde{\mathbf{b}}}_0 + \sum_{i=1}^{n-1} (\dot{\tilde{\mathbf{a}}}_i + \dot{\tilde{\mathbf{b}}}_i) + \dot{\tilde{\mathbf{a}}}_n \quad (40)$$

However,

$$\dot{\tilde{\mathbf{b}}}_i = \frac{d(\tilde{\mathbf{b}}_i)}{dt} = (\boldsymbol{\omega}_i \times \mathbf{A}_i) (\tilde{\mathbf{b}}_i) = \boldsymbol{\omega}_i \times \tilde{\mathbf{b}}_i. \quad (41)$$

Similarly,

$$\dot{\tilde{\mathbf{a}}}_i = \boldsymbol{\omega}_i \times \tilde{\mathbf{a}}_i. \quad (42)$$

Then, (40) can be further derived as

$$\tilde{\mathbf{v}}_e = \dot{\tilde{\mathbf{b}}}_0 + \sum_{i=1}^{n-1} (\dot{\tilde{\mathbf{a}}}_i + \dot{\tilde{\mathbf{b}}}_i) + \dot{\tilde{\mathbf{a}}}_n$$

$$= \boldsymbol{\omega}_0 \times \tilde{\mathbf{b}}_0 + \sum_{i=1}^{n-1} [\boldsymbol{\omega}_i \times (\tilde{\mathbf{a}}_i + \tilde{\mathbf{b}}_i)] + \boldsymbol{\omega}_n \times \tilde{\mathbf{a}}_n \quad (43)$$

where $\boldsymbol{\omega}_i$ is the angular velocities of B_i 's centroid. It can be calculated by the following:

$$\boldsymbol{\omega}_i = \boldsymbol{\omega}_0 + \sum_{k=1}^i k_k \dot{\theta}_k \quad (44)$$

Substituting (44) into (43), we obtain the following equation:

$$\begin{aligned} \tilde{\mathbf{v}}_e &= \boldsymbol{\omega}_0 \times \tilde{\mathbf{p}}_e + \sum_{k=1}^n [k_k \times (\tilde{\mathbf{p}}_e - \tilde{\mathbf{p}}_k)] \dot{\theta}_k \\ &= -\tilde{\mathbf{p}}_e \times \boldsymbol{\omega}_0 + \sum_{k=1}^n [k_k \times (\tilde{\mathbf{p}}_e - \tilde{\mathbf{p}}_k)] \dot{\theta}_k \\ &= -\tilde{\mathbf{p}}_e \times \boldsymbol{\omega}_0 + \tilde{\mathbf{J}}_{mv} \dot{\Theta} \end{aligned} \quad (45)$$

where

$$\tilde{\mathbf{J}}_{mv} = [k_1 \times (\tilde{\mathbf{p}}_e - \tilde{\mathbf{p}}_1) \dots k_n \times (\tilde{\mathbf{p}}_e - \tilde{\mathbf{p}}_n)] \in \mathbb{R}^{3 \times n} \quad (46)$$

According to (39) and (45), we get the following:

$$\mathbf{v}_0 = (\tilde{\mathbf{p}}_e \times \boldsymbol{\omega}_0 - \tilde{\mathbf{J}}_{mv} \dot{\Theta}) \quad (47)$$

Substituting (47) into (38), we can obtain the following:

$$\mathbf{H}_s \boldsymbol{\omega}_0 + \mathbf{H}_{\Theta} \dot{\Theta} = \mathbf{0} \quad (48)$$

where

$$\mathbf{H}_s = M \mathbf{r}_g \times \tilde{\mathbf{p}}_e \times + \mathbf{I}_w \quad (49)$$

$$\mathbf{H}_{\Theta} = \mathbf{I}_{\phi} - M \mathbf{r}_g \times \tilde{\mathbf{J}}_{mv} \quad (50)$$

2) *Coupling for Base Velocities:* According to (48), we can get

$$\boldsymbol{\omega}_0 = \mathbf{H}_s^{-1} \mathbf{H}_{\Theta} \dot{\Theta} = \mathbf{C}_{bj}^{\omega} \dot{\Theta} \quad (51)$$

where $\mathbf{C}_{bj}^{\omega} = \mathbf{H}_s^{-1} \mathbf{H}_{\Theta}$. Equation (51) establishes the relationship between the joint rates and the base's angular velocity. It reflects the coupling motion from the joint to the base's attitude. The coupling matrix is then denoted as \mathbf{C}_{bj}^{ω} , where the subscript bj means from joint j to base b attitude and the superscript ω denotes the angular velocity. This type of coupling is called joint-to-base rotation coupling.

Substituting (51) to (47), the linear velocity of the base is obtained as follows:

$$\mathbf{v}_0 = (\tilde{\mathbf{p}}_e \times \boldsymbol{\omega}_0 - \tilde{\mathbf{J}}_{mv} \dot{\Theta}) = (\tilde{\mathbf{p}}_e \times \mathbf{C}_{bj}^{\omega} - \tilde{\mathbf{J}}_{mv}) \dot{\Theta} = \mathbf{C}_{bj}^v \dot{\Theta} \quad (52)$$

where $\mathbf{C}_{bj}^v = (\tilde{\mathbf{p}}_e \times \mathbf{C}_{bj}^{\omega} - \tilde{\mathbf{J}}_{mv})$ establishes the relationship between the joint rates and the base's linear velocity. This coupling is called joint-to-base translation coupling. We can see that \mathbf{C}_{bj}^v depends on \mathbf{C}_{bj}^{ω} .

Equations (51) and (52) can be combined into the following form:

$$\begin{bmatrix} \mathbf{v}_0 \\ \boldsymbol{\omega}_0 \end{bmatrix} = \begin{bmatrix} \mathbf{C}_{bj}^v \\ \mathbf{C}_{bj}^\omega \end{bmatrix} \dot{\Theta} = \mathbf{C}_{bj} \dot{\Theta} \quad (53)$$

Here, the matrix \mathbf{C}_{bj} is called the joint-to-base coupling matrix. Substituting (53) to (1), we get the following equation:

$$\begin{bmatrix} \mathbf{v}_e \\ \boldsymbol{\omega}_e \end{bmatrix} = \mathbf{J}_b \begin{bmatrix} \mathbf{v}_0 \\ \boldsymbol{\omega}_0 \end{bmatrix} + \mathbf{J}_m \dot{\Theta} = [\mathbf{J}_b \mathbf{C}_{bj} + \mathbf{J}_m] \dot{\Theta} = \mathbf{J}_g \dot{\Theta} \quad (54)$$

where $\mathbf{J}_g = \mathbf{J}_b \mathbf{C}_{bj} + \mathbf{J}_m$ is the so-called GJM [18]. If \mathbf{J}_g is a nonsingular square matrix, the joint rates can be calculated from (54):

$$\dot{\Theta} = \mathbf{J}_g^{-1} \begin{bmatrix} \mathbf{v}_e \\ \boldsymbol{\omega}_e \end{bmatrix} = [\mathbf{J}_b \mathbf{C}_{bj} + \mathbf{J}_m]^{-1} \begin{bmatrix} \mathbf{v}_e \\ \boldsymbol{\omega}_e \end{bmatrix} \quad (55)$$

Substituting (55) into (51) and (52), we can obtain the coupling motion from the end velocities to the base angular and linear velocities, respectively:

$$\boldsymbol{\omega}_0 = \mathbf{C}_{bj}^\omega \dot{\Theta} = \mathbf{C}_{bj}^\omega \mathbf{J}_g^{-1} \dot{\mathbf{x}}_e = \mathbf{C}_{be}^\omega \dot{\mathbf{x}}_e \quad (56)$$

$$\mathbf{v}_0 = \mathbf{C}_{bj}^v \dot{\Theta} = \mathbf{C}_{bj}^v \mathbf{J}_g^{-1} \dot{\mathbf{x}}_e = \mathbf{C}_{be}^v \dot{\mathbf{x}}_e \quad (57)$$

where $\mathbf{C}_{be}^\omega = \mathbf{C}_{bj}^\omega \mathbf{J}_g^{-1}$ and $\mathbf{C}_{be}^v = \mathbf{C}_{bj}^v \mathbf{J}_g^{-1}$ establish the relationship between the end velocities and the base's angular and linear velocities, respectively. These two types of coupling are called end-to-base rotation coupling and end-to-base translation coupling, respectively.

A combined equation is then obtained from (56) and (57):

$$\begin{bmatrix} \mathbf{v}_0 \\ \boldsymbol{\omega}_0 \end{bmatrix} = \begin{bmatrix} \mathbf{C}_{be}^v \\ \mathbf{C}_{be}^\omega \end{bmatrix} \dot{\mathbf{x}}_e = \mathbf{C}_{be} \dot{\mathbf{x}}_e \quad (58)$$

The matrix \mathbf{C}_{be} is called the end-to-base coupling matrix. It is easy to find that $\mathbf{C}_{be} = \mathbf{C}_{bj} \mathbf{J}_g^{-1}$.

IV. DYNAMIC COUPLING FACTORS

A. The Coupling Factor of the Base Centroid Position

Base on (17), we get the position of end-effector of the space manipulator as follows:

$$\mathbf{p}_e = \mathbf{r}_g + \hat{\mathbf{b}}_0 + \sum_{i=1}^n (\hat{\mathbf{a}}_i + \hat{\mathbf{b}}_i) \quad (59)$$

where

$$\begin{cases} \hat{\mathbf{a}}_i = \frac{\sum_{q=0}^{i-1} m_q}{M} \mathbf{a}_i, i = 1, \dots, n \\ \hat{\mathbf{b}}_i = \frac{\sum_{q=0}^i m_q}{M} \mathbf{b}_i, i = 0, \dots, n \end{cases} \quad (60)$$

Vectors $\hat{\mathbf{a}}_i$ and $\hat{\mathbf{b}}_i$ are the virtual link vectors of the VM model [16]. The maximum RWS of the VM is a sphere. Its

center is the system CM , i.e., $\mathbf{O}_{\text{RWS}} = \mathbf{r}_g$, and the radius is as follows [32]:

$$\begin{aligned} R_{\text{RWS}} &= \max_{\Theta} (\|\mathbf{p}_e\|) \\ &= \max_{\theta_0, \theta_i \in [-\pi, \pi]} \left(\left\| \mathbf{A}_0 \left[{}^0 \hat{\mathbf{b}}_0 + \sum_{i=1}^n {}^0 \mathbf{A}_i \left({}^i \hat{\mathbf{a}}_i + {}^i \hat{\mathbf{b}}_i \right) \right] \right\| \right) \\ &= \max_{\theta_i \in [-\pi, \pi]} \left(\left\| {}^0 \hat{\mathbf{b}}_0 + \sum_{i=1}^n {}^0 \mathbf{A}_i \left({}^i \hat{\mathbf{a}}_i + {}^i \hat{\mathbf{b}}_i \right) \right\| \right) \end{aligned} \quad (61)$$

Similarly, we can derive the CWS and the FWS of the VM. The radiiuses are denoted as R_{CWS} and R_{FWS} , respectively [32].

According to the definition, the position of the VM's end-effector is the same as that of the real space manipulator's end-effector, and the position of the BCVM's end-effector reflects that of the base's centroid. Therefore, we can use the radius ratio of the coupled space and the workspace to measure the degree of the coupling for the base centroid position. Corresponding to different types of coupled space and workspace, the following ratios are defined for different requirements:

$$\sigma_R = \frac{R_{\text{RCS}}}{R_{\text{RWS}}} \quad (62)$$

$$\sigma_C = \frac{R_{\text{CCS}}}{R_{\text{CWS}}} \quad (63)$$

$$\sigma_F = \frac{R_{\text{FCS}}}{R_{\text{FWS}}} \quad (64)$$

B. The Coupling Factor of the Base Rotation Coupling

According to the preceding derivation, the coupling matrices \mathbf{C}_{bj}^ω , \mathbf{C}_{bj}^v , \mathbf{C}_{be}^ω , and \mathbf{C}_{be}^v are the functions of the mass properties (including the mass, inertia, and centroid position) of each body of the space robotic system, the attitude of the base, and the joint angles of the manipulator. The corresponding coupling degrees can be analyzed using these matrices.

The preceding derivation also shows that the translation coupling motion depends on the rotation coupling motion. Therefore, we focus on analyzing the rotation coupling of the base, including joint-to-base and end-to-base rotation coupling motion.

1) *Joint-to-Base Rotation Coupling Factor*: The joint-to-base rotation coupling is represented as (51). Then, the ratio between the base angular velocity and the joint rates is defined as the corresponding coupling factor. The expression is as follows:

$$w_{bj}^\omega(\dot{\Theta}) = \frac{|\omega_0|_2}{|\dot{\Theta}|_2} = \frac{\langle \mathbf{C}_{bj}^\omega \dot{\Theta}, \mathbf{C}_{bj}^\omega \dot{\Theta} \rangle^{1/2}}{\langle \dot{\Theta}, \dot{\Theta} \rangle^{1/2}} = \sqrt{\frac{\dot{\Theta}^T \mathbf{A}_{bj}^\omega \dot{\Theta}}{\dot{\Theta}^T \dot{\Theta}}} \quad (65)$$

where w_{bj}^ω describes the variation degree of the base attitude caused by the given joint motion; $|\cdot|_2$ defines the 2-norm of the vector; and $\mathbf{A}_{bj}^\omega = (\mathbf{C}_{bj}^\omega)^T \mathbf{C}_{bj}^\omega$ is a n -order real symmetric square. Assuming that $\lambda_1, \dots, \lambda_n$

TABLE III
Parameters of Virtual Links

Length	${}^0\hat{\mathbf{b}}_0/{}^0\tilde{\mathbf{b}}_0$ (m)	${}^1\mathbf{a}_1$ (m)	${}^1\mathbf{b}_1$ (m)	${}^2\mathbf{a}_2$ (m)	${}^2\mathbf{b}_2$ (m)
VM	0.6000	0	0.5820	0	0.6305
BCVM	0.4000	0	0.3880	0	0.3395

($0 \leq \lambda_1 \leq \dots \leq \lambda_n$) are the eigenvalues of the matrix \mathbf{A}_{bj}^ω and $\mathbf{p}_1, \dots, \mathbf{p}_n$ are the corresponding orthonormal eigenvectors, the joint-to-base dynamic coupling factor satisfies the following inequality:

$$\sqrt{\lambda_1(\mathbf{A}_{bj}^\omega)} \leq w_{bj}^\omega(\dot{\Theta}) \leq \sqrt{\lambda_n(\mathbf{A}_{bj}^\omega)} \quad (66)$$

where

$$\lambda_1(\mathbf{A}_{bj}^\omega) = (w_{bj}^\omega(\dot{\Theta}))_{\min} = w_{bj}^\omega(\dot{\Theta})|_{\dot{\Theta}=\mathbf{p}_1} \quad (67)$$

$$\lambda_n(\mathbf{A}_{bj}^\omega) = (w_{bj}^\omega(\dot{\Theta}))_{\max} = w_{bj}^\omega(\dot{\Theta})|_{\dot{\Theta}=\mathbf{p}_n} \quad (68)$$

2) *End-to-Base Rotation Coupling Factor*: Similar to the preceding factor, the ratio between the base's angular velocity and the end-effector velocity can be determined by the following:

$$w_{be}^\omega(\dot{\mathbf{x}}_e) = \frac{|\omega_0|_2}{|\dot{\mathbf{x}}_e|_2} = \frac{\langle \mathbf{C}_{be}^\omega \dot{\mathbf{x}}_e, \mathbf{C}_{be}^\omega \dot{\mathbf{x}}_e \rangle^{1/2}}{\langle \dot{\mathbf{x}}_e, \dot{\mathbf{x}}_e \rangle^{1/2}} = \sqrt{\frac{\dot{\mathbf{x}}_e^T \mathbf{A}_{be}^\omega \dot{\mathbf{x}}_e}{\dot{\mathbf{x}}_e^T \dot{\mathbf{x}}_e}} \quad (69)$$

where w_{be}^ω represents the variation extent of the base attitude generated by end-effector motion. Hence, it is taken as a coupling factor to measure the dynamic effect on the base's attitude from the end-effector. Because $\mathbf{C}_{be}^\omega = \mathbf{C}_{bj}^\omega \mathbf{J}^{-1} \in \mathbb{R}^{3 \times 6}$, $\mathbf{A}_{be}^\omega = (\mathbf{C}_{be}^\omega)^T \mathbf{C}_{be}^\omega$ is a 6×6 real symmetric square.

The end-to-base dynamic coupling factor $w_{be}^\omega(\dot{\mathbf{x}}_e)$ satisfies the following inequality:

$$\sqrt{\lambda_1(\mathbf{A}_{be}^\omega)} \leq w_{be}^\omega(\dot{\mathbf{x}}_e) \leq \sqrt{\lambda_6(\mathbf{A}_{be}^\omega)} \quad (70)$$

where $0 \leq \lambda_1 \leq \lambda_2 \leq \dots \leq \lambda_6$ are the eigenvalues of the matrix \mathbf{A}_{be}^ω and $\mathbf{p}_1, \mathbf{p}_2, \dots, \mathbf{p}_6$ are the corresponding eigenvectors.

V. DYNAMIC COUPLING ANALYSIS

For practical applications, such as designing a new manipulator or using an existing robotic system, it is important to analyze the dynamic coupling between the manipulator (joint or end-effector) and the base. The main analysis includes the coupling degree about different loads, installation positions, and joint configurations. Based on the hybrid method, we can analyze the coupling between the base centroid position and the attitude.

A. A Planar Space Robotic System

A planar space robotic system (Fig. 5) is taken as an example. The mass properties of the robotic system are shown in Table II. The normal configuration for the

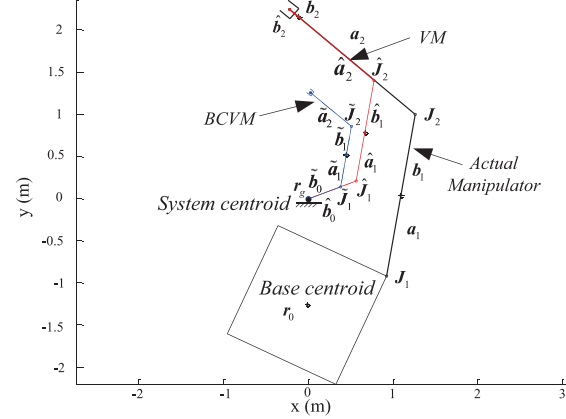


Fig. 6. BCVM and VM models of planar space robotic system.

coupling analysis is defined as $\theta_0 = 20^\circ$, $\theta_1 = 60^\circ$, and $\theta_2 = 60^\circ$, where θ_0 is the attitude of the base and θ_1 and θ_2 are the two joint variables. The installation pose is determined by a constant angle φ . The virtual link parameters of the BCVM and VM are shown in Table III. The inertial frame is located at the system's centroid, so $\mathbf{r}_g = 0$. The configurations of the BCVM and VM are shown in Fig. 6.

B. Dynamic Coupling Analysis for Different Load Mass

When a target is captured by the space robot, the end-effector and the captured target (the payload of the manipulator) form a new link. The mass, centroid position vector and moment of inertia of the payload are denoted by m_L , \mathbf{r}_L , and \mathbf{I}_L .

The equivalent mass of the new end link is determined by the following:

$$\tilde{m}_n = m_n + m_L \quad (71)$$

The position vector of the equivalent centroid is as follows:

$$\tilde{\mathbf{r}}_n = (m_n \mathbf{r}_n + m_L \mathbf{r}_L) / (m_n + m_L) \quad (72)$$

According to the parallel axis theorem, the moment of inertia of the combined link is defined as follows:

$$\begin{aligned} \tilde{\mathbf{I}}_n &= \mathbf{I}_n + m_n (\mathbf{r}_n^T \mathbf{r}_n \mathbf{E} - \mathbf{r}_n \mathbf{r}_n^T) + \mathbf{I}_L \\ &\quad + m_L (\mathbf{r}_L^T \mathbf{r}_L \mathbf{E} - \mathbf{r}_L \mathbf{r}_L^T) \end{aligned} \quad (73)$$

1) *Base Centroid Coupling Analysis*: In this part, we investigate the effects of the load mass on the reachable workspace and the maximum coupled space. Four typical cases are studied: $m_L = 0$ kg (without payload),

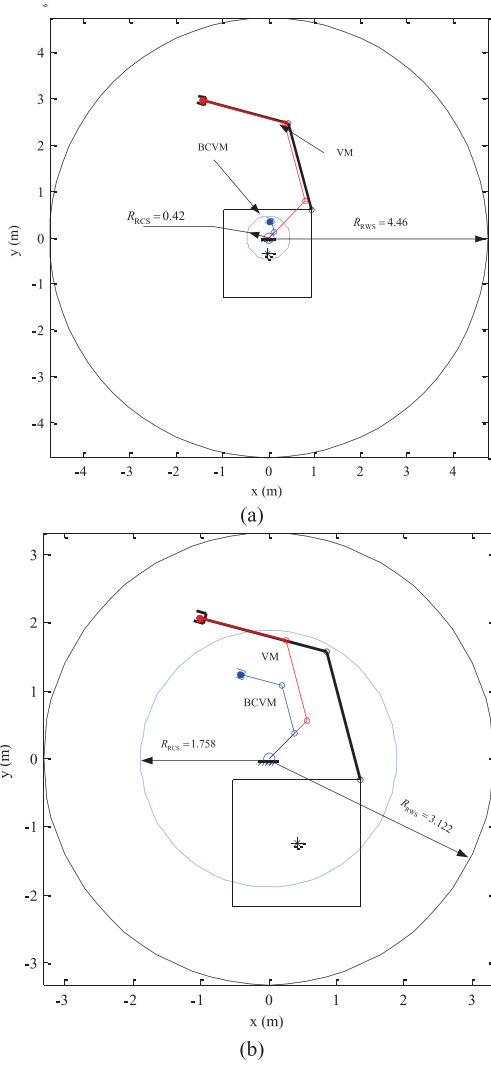


Fig. 7. Reachable workspace and coupled space vs. different load masses. (a) $m_L = 50 \text{ kg}$. (b) $m_L = 150 \text{ kg}$.

$m_L = 50 \text{ kg}$, $m_L = 100 \text{ kg}$, and $m_L = 150 \text{ kg}$. The equivalent mass, centroid position, and moment of inertia are calculated according to (71), (72), and (73), respectively. The calculated workspace and coupled space corresponding to different load masses are shown in Fig. 7. Limited by paper length, we only give the results of $m_L = 0 \text{ kg}$ and $m_L = 150 \text{ kg}$. We can see that the coupled space becomes increasingly bigger as the load mass increases. It conforms to the actual situation. Based on the analysis, we can evaluate the payload manipulation ability for a space robotic system. For a given mission, the coupled motion trajectory can be further analyzed. For example, if the space manipulator is driven to move a 150-kg payload (i.e., $m_L = 150 \text{ kg}$) along a circle, the corresponding trajectories of the real manipulator, the BCVM, and the base centroid can be determined. They are shown in Fig. 8.

2) Base Attitude Coupling Analysis: Sometimes, the possible variation of the base attitude is the key for the on-orbit mission. Here, we analyze the attitude coupling

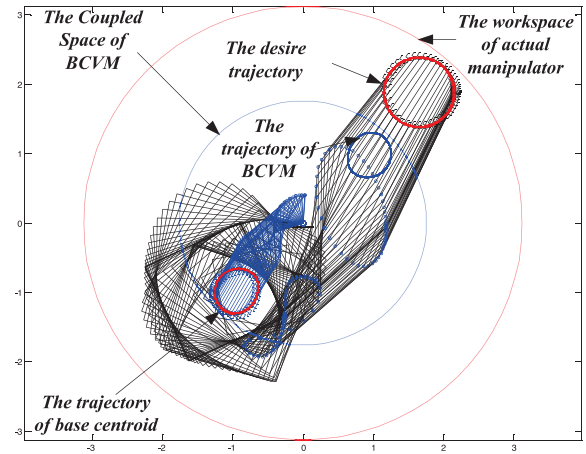


Fig. 8. Coupled trajectory analysis for $m_L = 150 \text{ kg}$.

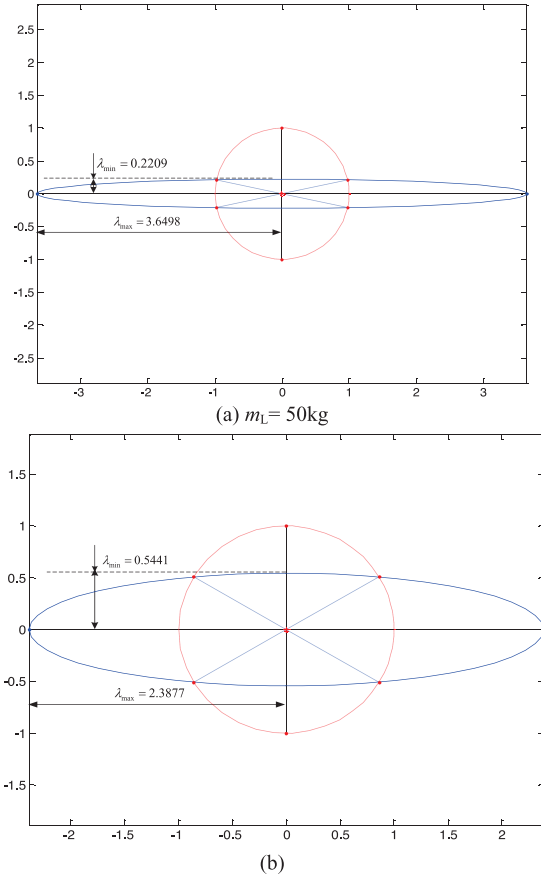
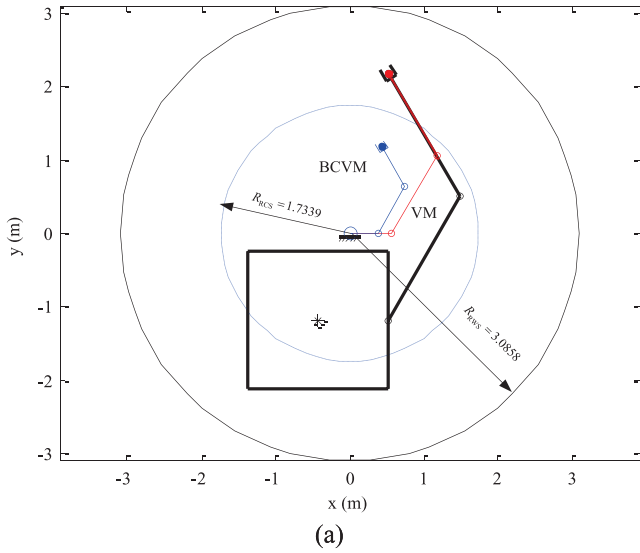


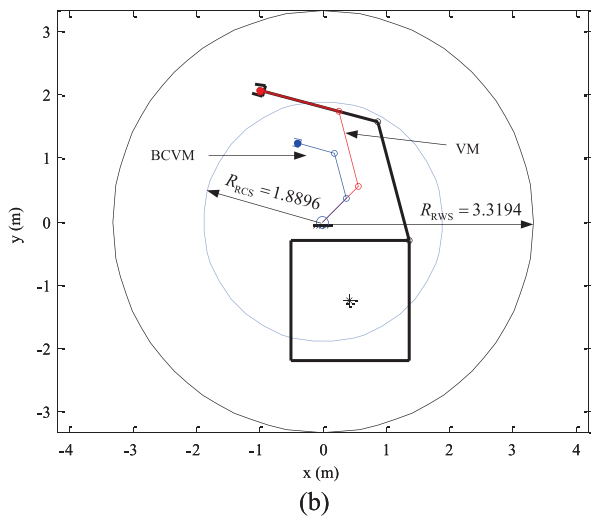
Fig. 9. Attitude coupling analysis for different load masses. (a) $m_L = 50 \text{ kg}$. (b) $m_L = 150 \text{ kg}$.

motion for different payloads. Assuming that the module of the end-effector velocity is 1, we can calculate the maximum and minimum end-to-base rotation coupling factors.

For the four typical cases, i.e., $m_L = 0 \text{ kg}$ (without load), $m_L = 50 \text{ kg}$, $m_L = 100 \text{ kg}$, and $m_L = 150 \text{ kg}$, the analysis results are shown in Fig. 9. Limited by paper length, we only give the results of $m_L = 50 \text{ kg}$ and $m_L = 150 \text{ kg}$. We can see that the bigger the mass of the load, the bigger the attitude variable of the base. The



(a)



(b)

Fig. 10. Reachable workspace of VM and coupled space of BCVM varies with installation pose. (a) $\varphi = 0$. (b) $\varphi = 45^\circ$.

analysis is also useful to evaluate the payload manipulation ability for a space robotic system.

C. Dynamic Coupling Analysis for Installation Pose

In this part, we analyze the dynamic coupling for different installation poses. Here, the angle φ is used to determine the mounted position of the space manipulator.

1) *Base Centroid Coupling Analysis*: The mass of the captured payload is assumed to be 150 kg. According to the simulation results, the reachable workspace and the maximum coupled space are shown in Fig. 10, corresponding to $\varphi = 0^\circ$ and $\varphi = 45^\circ$, respectively. The other cases are also analyzed. Limited by the length of the paper, we only give the details of the two preceding cases. The base centroid coupling factor is also calculated corresponding to different installation angles. The result is shown as Fig. 11. We can see that the maximum coupling occurs when $\varphi = 45^\circ$ and the minimum coupling occurs

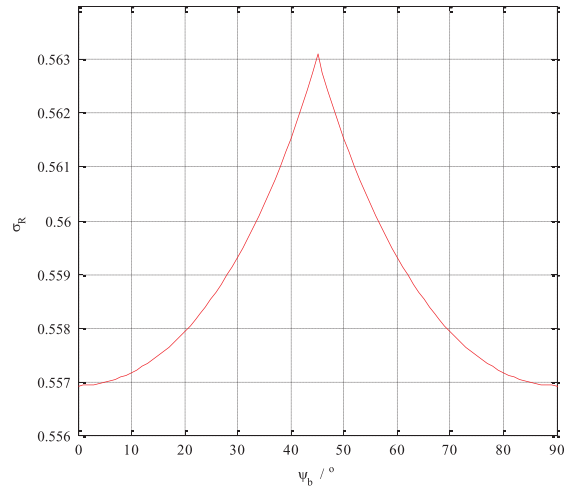
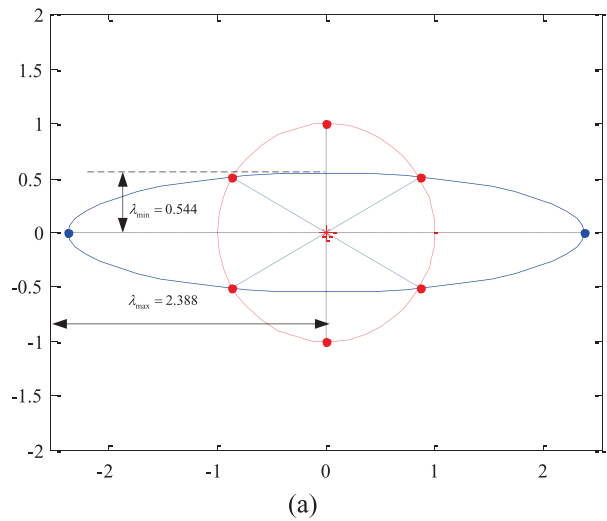
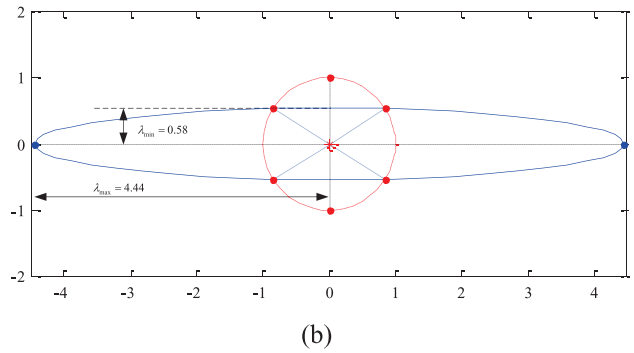


Fig. 11. Centroid position coupling factor vs. installation pose.



(a)



(b)

Fig. 12. Base-to-end rotation coupling vs. installation pose. (a) $\varphi = 0$. (b) $\varphi = 45^\circ$.

when $\varphi = 0^\circ$ or $\varphi = 90^\circ$. This result is useful for practical application.

2) *Analysis for Base Attitude*: As in the preceding section, we can analyze the attitude coupling for different installation angles. The results corresponding to $\varphi = 0^\circ$ and $\varphi = 45^\circ$ are shown in Fig. 12. This analysis supplies useful information to design the installation angle of a space manipulator or evaluate the disturbance on the base's attitude for a given installation angle.

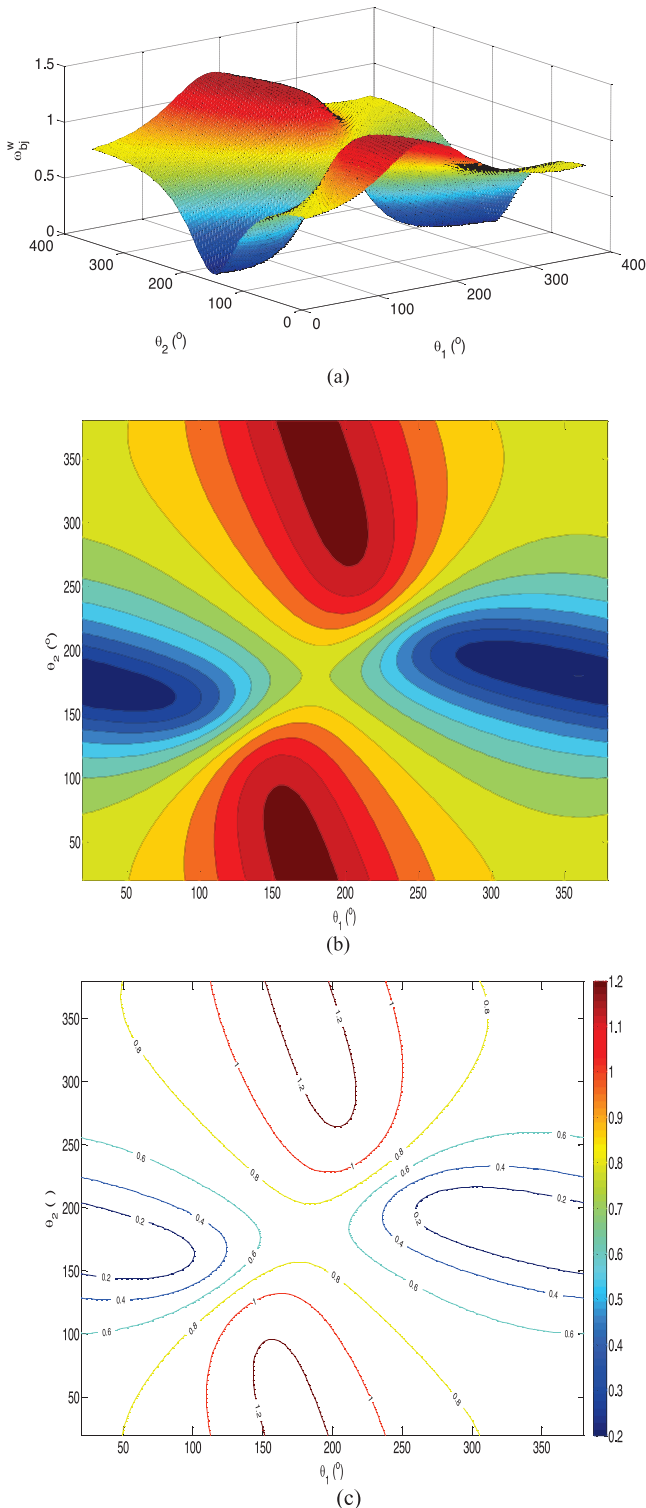


Fig. 13. Joint-to-base rotation coupling map with $m_L = 50$ kg. (a) Joint-to-base coupling map in 3D form. (b) Joint-to-base coupling map in 2D form. (c) Contour line of joint-to-base coupling map.

D. Coupling Maps

Because of the nonholonomic characteristic, different joint trajectories cause different variation of the base's attitude. The enhanced disturbance map [33] was used to plan the path for minimizing the spacecraft attitude

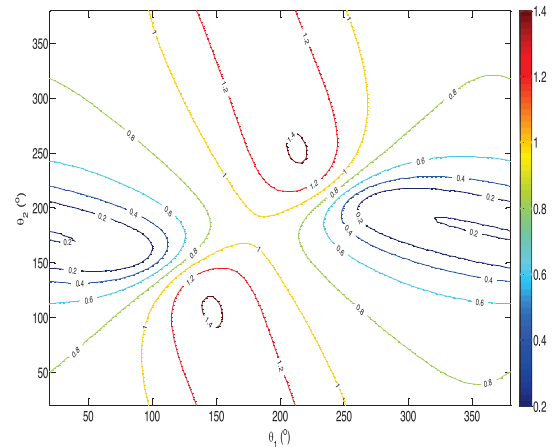


Fig. 14. Joint-to-base rotation coupling map with $m_L = 150$ kg.

disturbance. The reaction null space methods were also used for some cases [34, 35]. Based on the presented dynamic coupling model, the joint-to-base and end-to-base coupling maps are easily established and can be used to plan the trajectory of the space manipulator for minimizing attitude disturbance effectively.

1) *Joint-to-Base Coupling Map:* The coupling map is defined as the drawing including all possible values of the coupling factor about the joint configuration. According to (65), the joint-to-base rotation coupling map can be established. Taking the planar space robotic system introduced in section V.A as the example, the coupling maps corresponding to $m_L = 50$ kg and $m_L = 150$ kg are shown in Figs. 13 and 14, respectively. The subplot in Fig. 13(a) denotes the 3D form of the coupling map, the subplot in Fig. 13(b) is the corresponding 2D form, and the subplot in Fig. 13(c) is the contour line. Based on the coupling maps, it is easy to find the areas with high or low disturbance on the spacecraft attitude caused by the joint velocities. This is important for the practical application. The coupling maps provide theoretical guidance to plan the suitable trajectory of the space robot to perform on-orbit tasks.

2) *End-to-Base Coupling Map:* Similarly, the end-to-base coupling maps can be established according to (69), which defines the coupling factor w_{be}^ω . For the two cases $m_L = 50$ kg and $m_L = 150$ kg, the results are shown in Figs. 15 and 16, respectively. The coupling maps show the high or low disturbance on the base attitude caused by the end-effector's velocities.

VI. CONCLUSION

Because of dynamic coupling, the motion of a manipulator alters the position and attitude of the base; furthermore, the end-effectors lose the desired target pose because of the motion of the base. It complicates the trajectory planning and control of a space robotic system. According to different characteristics of the linear and angular momentum conservation equations, a hybrid method is proposed to model dynamic coupling and define

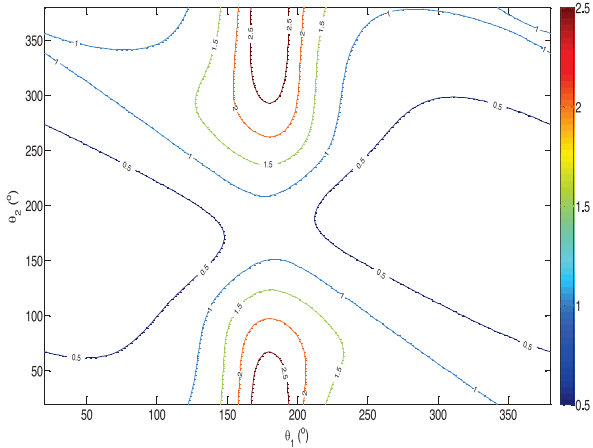


Fig. 15. End-to-base coupling map with $m_L = 50 \text{ kg}$.

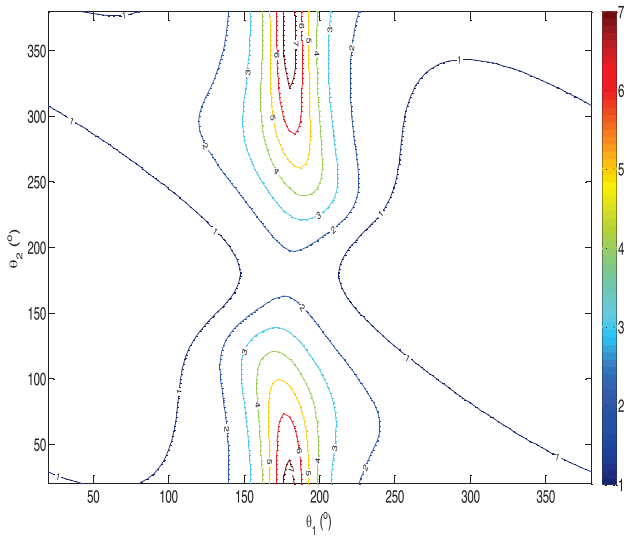


Fig. 16. End-to-base coupling map with $m_L = 150 \text{ kg}$.

the corresponding coupling factors. The coupling effect on the base centroid generated by the manipulator is analyzed at the position level, directly reflecting the position relationship and avoiding the singularity existing for differential equations resolving. The variation range of the base centroid is determined according to the workspace of the BCVM. However, the coupling motion of the base attitude is derived by solving the angular momentum conservation and eliminating the holonomic constraints. The coupling effect on the motion of the base is classified into joint-to-base and end-to-base rotation–translation coupling types.

Different from previous works, we derived the relationship between the rotation and the translation coupling equations and revealed the coupled translation motion dependence on rotation motion. Based on the decomposition, each subtype of coupling motion can be separately analyzed for different requirements. The coupling factors corresponding to the position-level and velocity-level models are then defined to measure the coupling. Using the presented model, we analyzed the

dynamic coupling for different loads, installation positions, and joint configurations. The coupling maps were also established to illustrate the coupling effects clearly. This work is useful for practical applications, such as designing a new manipulator or using an existing robotic system. In the future, we will study the optimal design of a space manipulator to reduce the dynamic coupling and the trajectory planning and dynamic control methods based on the proposed coupling models, coupling factors, and coupling maps.

REFERENCES

- [1] Badavi, F. F.
Exposure estimates for repair satellites at geosynchronous orbit.
Acta Astronautica, **83** (2013), 18–26.
- [2] White, A. E., and Lewis, H. G.
The many futures of active debris removal.
Acta Astronautica, **95** (2014), 189–197.
- [3] Liu, X., Baoyin, H., and Ma, X.
Optimal path planning of redundant free-floating revolute-jointed space manipulators with seven links.
Multibody System Dynamics, **29**, 1 (2013), 41–56.
- [4] Ellery, A., Kreisel, J., and Sommer, B.
The case for robotic on-orbit servicing of spacecraft: Spacecraft reliability is a myth.
Acta Astronautica, **63**, 5–6 (2008), 632–648.
- [5] Flores-Abad, A., Ma, O., Pham, K., and Ulrich, S.
A review of space robotics technologies for on-orbit servicing.
Progress in Aerospace Sciences, **68** (2014), 1–26.
- [6] Kimura, S., Okuyama, T., Yoshioka, N., and Wakabayashi, Y.
Robot-aided remote inspection experiment on STS-85.
IEEE Transactions on Aerospace and Electronic Systems, **36**, 4 (2000), 1290–1297.
- [7] Zhang, J., Zhao, S., and Yang, Y.
Characteristic analysis for elliptical orbit hovering based on relative dynamics.
IEEE Transactions on Aerospace and Electronic Systems, **49**, 4 (2013), 2742–2750.
- [8] Segal, S., Gurfil, P., and Shahid, K.
In-orbit tracking of resident space objects: A comparison of monocular and stereoscopic vision.
IEEE Transactions on Aerospace and Electronic Systems, **50**, 1 (2014), 676–688.
- [9] Li, Y., Jing, Z., and Liu, G.
Maneuver-aided active satellite tracking using six-DOF optimal dynamic inversion control.
IEEE Transactions on Aerospace and Electronic Systems, **50**, 1 (2014), 704–719.
- [10] Xu, Y., Shum, H. Y., Kanade, T., and Lee, J.
Parameterization and adaptive control of space robot systems.
IEEE Transactions on Aerospace and Electronic Systems, **40** (1994), 435–451.
- [11] Wang, H., and Xie, Y.
Prediction error based adaptive Jacobian tracking for free-floating space manipulators.
IEEE Transactions on Aerospace and Electronic Systems, **48**, 4 (2012), 3207–3221.
- [12] Papadopoulos, E., and Dubowsky, S.
On the nature of control algorithms for free-floating space manipulators.
IEEE Transactions on Robotics and Automation, **7**, 6 (1991), 750–758.
- [13] Papadopoulos, E., Tortopidis, I., and Nanos, K.
Smooth planning for free-floating space robots using polynomials.

- [14] Huang, Y. In *Proceedings of the IEEE International Conference on Robotics and Automation*, Barcelona, Spain, 2005, 4272–4277.
- [15] Ma, O., Buhariwala, K., Neil, R., Maclean, J., and Carr, R. MDSF: A generic development and simulation facility for flexible, complex robotic systems. *Robotica*, **15**, 1 (1997), 49–62.
- [16] Vafa, Z., and Dubowsky, S. The kinematics and dynamics of space manipulators: The virtual manipulator approach. *The International Journal of Robotics Research*, **9**, 4 (1990), 3–21.
- [17] Liang, B., Xu, Y. S., and Bergerman, M. Mapping a free-floating space manipulator to a dynamically equivalent manipulators. *ASME Transactions on Dynamics, Measurement, and Control*, **120** (1998), 1–7.
- [18] Umetani, Y., and Yoshida, K. Resolved motion rate control of space manipulators with generalized Jacobian matrix. *IEEE Transactions on Robotics and Automation*, **5**, 3 (1989), 303–314.
- [19] Nakamura, Y., and Mukherjee, R. Nonholonomic path planning of space robots via a bidirectional approach. *IEEE Transactions on Robotics and Automation*, **7**, 4 (1991), 500–514.
- [20] Yoshida, K., Hashizume, K., and Abiko, S. Zero reaction maneuver: Flight validation with ETS-VII space robot and extension to kinematically redundant arm. In *Proceedings of the IEEE International Conference on Robotics and Automation*, Piscataway, NJ, 2001, 441–446.
- [21] Yoshida, K. Engineering test satellite VII flight experiments for space robot dynamics and control: Theories on laboratory test beds ten years ago, now in orbit. *International Journal of Robotics Research*, **22**, 5 (2003), 321–335.
- [22] Xu, W., Li, C., Wang, X., Liang, B., Liu, Y., and Xu, Y. Study on non-holonomic cartesian path planning of free-floating space robotic system. *Advanced Robotics*, **23**, 1–2 (2009), 113–143.
- [23] Xu, W., Liu, Y., Liang, B., Wang, X., and Xu, Y. Unified multi-domain modeling and simulation of space robot for capturing a moving target. *Multibody System Dynamics*, **23**, 3 (2010), 293–331.
- [24] Xu, Y., and Shum, H.
- [25] Bergerman, M., Lee, C., and Xu, Y. Dynamic control and coupling of a free-flying space robot system. *Journal of Robotic Systems*, **11**, 7 (1994), 573–589.
- [26] Bergerman, M., Lee, C., and Xu, Y. Dynamic coupling of underactuated manipulators. In *Proceedings of the 4th IEEE Conference on Control Applications*, Albany, NY, 1995, 500–505.
- [27] Bergerman, M., Lee, C., and Xu, Y. A dynamic coupling index for underactuated manipulators. *Journal of Robotic Systems*, **12**, 10 (1995), 693–707.
- [28] Carignan, C. R., and Akin, D. L. The reaction stabilization of on-orbit robots. *IEEE Control Systems Magazine*, **20**, 6 (2000), 19–33.
- [29] Toglia, C., Sabatini, M., Gasbarri, P., and Palmerini, G. B. Optimal target grasping of a flexible space manipulator for a class of objectives. *Acta Astronautica*, **68**, 7–8 (2011), 1031–1041.
- [30] Carter, F. M., and Cherchas, D. B. Motion control of non-fixed base robotic manipulators. *Robotica*, **17**, 2 (1999), 143–157.
- [31] Chung, W. K., Qian, H., Lam, T. L., and Xu, Y. Novel design of gaits on space station for dynamic disturbance minimization. *IEEE/ASME Transactions on Mechatronics*, **19**, 4 (2014), 1392–1403.
- [32] Ellery, A. An engineering approach to the dynamic control of space robotic on-orbit servicers. In *Proceedings of the Institution of Mechanical Engineers, Part G: Journal of Aerospace Engineering*, **218**, 4 (2004), 79–98.
- [33] Dubowskys, S., and Torres, M. Path planning for space manipulators to minimizing spacecraft attitude disturbance. In *Proceedings of the IEEE International Conference on Robotics and Automation*, Sacramento, CA, 1991, 2522–2528.
- [34] Nenchev, D. N., Yoshida, K., Vichitkulsawat, P., and Uchiyama, M. Reaction null-space control of flexible structure mounted manipulator systems. *IEEE Transactions On Robotics And Automation*, **15**, 6 (1999), 1011–1023.
- [35] Piersigilli, P., Sharf, I., and Misra, A. K. Reactionless capture of a satellite by a two degree-of-freedom manipulator. *Acta Astronautica*, **66**, 1–2 (2010), 183–192.



Wenfu Xu (M'13) received a B.E. degree in 2001 and an M.E. degree in 2003, both in control engineering, from Hefei University of Technology, Hefei, China, and Ph.D. degrees in the control science and engineering from Harbin Institute of Technology, Harbin, China, in 2007. He was a research associate (as a visiting scholar) from February 2013 to February 2014 with the Department of Mechanical and Automation Engineering, The Chinese University of Hong Kong, Hong Kong, China.

He is a professor with the Department of Mechanical and Automation Engineering, Harbin Institute of Technology Shenzhen Graduate School, Shenzhen, China. His research interests include space robotics and multibody system dynamic and redundant manipulators.



Jianqing Peng received a B.E. degree in mechatronics engineering from Huazhong Agricultural University, Wuhan, Hubei, China, in 2012 and an M.E. degree in mechatronics engineering from Harbin Institute of Technology Shenzhen Graduate School, Shenzhen, China, in 2014.

He is working toward a Ph.D. degree at the Department of Mechatronics and Automation, Harbin Institute of Technology Shenzhen Graduate School, Shenzhen, China. His research interests include space robotics and multibody system dynamic and image processing.



Bin Liang (M'97) received B.S. and M.S. degrees in control engineering from Northwestern Polytechnical University, Xi An, China, in 1991 and 1994, respectively, and a Ph.D degree in precision instrument and mechanology from Tsinghua University, Beijing, China, in 1994.

He is a professor with the Department of Automation, Tsinghua University, Beijing, China. His research interests include space robotics, manipulators, and intelligent control.



Zonggao Mu received a B.E. degree in mechatronics engineering from Shandong University of Science and Technology, Qingdao, Shandong, China, in 2011 and an M.E. degree in mechatronics engineering from Harbin Institute of Technology Shenzhen Graduate School, Shenzhen, China, in 2013.

He is working toward a Ph.D. degree at the Department of Mechatronics and Automation, Harbin Institute of Technology Shenzhen Graduate School, Shenzhen, China. He is also an engineer working at Aerospace Dongfanghong Development, Shenzhen, China. His research interests include space robotics and redundant manipulators.